EurJIC European Journal of Inorganic Chemistry

ChemPubSoc Europe

Copper Complexes

Keywords: O ligands / Copper / Structure elucidation / Photoelectron spectroscopy / Bridging ligands

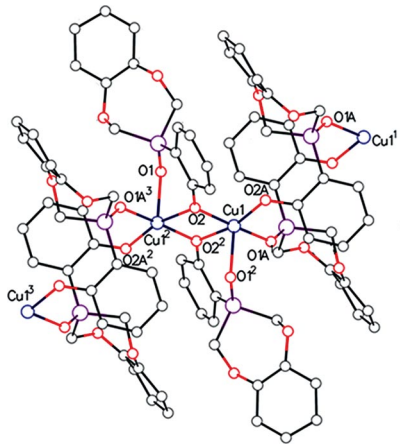

The formation of copper complexes with aromatic *o*-phosphorylated phenolates with both chelating and bridging configurations was demonstrated by single-crystal and powder X-ray diffraction. Photoelectron spectroscopy was utilized to reveal the coordination polyhedra around the copper ions in an amorphous copper complex.

EurJIC European Journal of Inorganic Chemistry

www.eurjic.org FULL PAPER

DOI:10.1002/ejic.201300540

Copper(II) Complexes with Aromatic *o*-Phosphorylated Phenols – Synthesis, Crystal Structures, and X-ray Photoelectron Spectroscopy

Sergey Shuvaev,*[a] Ivan S. Bushmarinov,[b] Ilya Sinev,[c] Artem O. Dmitrienko,[b] Konstantin A. Lyssenko,[b] Vladimir Baulin,[d,e] Wolfgang Grünert,[c] Aslan Yu. Tsivadze,[e] and Natalia Kuzmina[a]

Keywords: O ligands / Copper / Structure elucidation / Photoelectron spectroscopy / Bridging ligands

The structural properties of copper complexes with (2-hydroxyphenyl)di-*p*-tolylphosphane oxide ($Cu\mathbf{L^1}_2$) and 3-(2-hydroxyphenyl)-3,4-dihydro-2*H*-benzo[*f*][1,5,3]dioxaphosphepine 3-oxide ($Cu\mathbf{L^2}_2$) are studied in detail. The *o*-phosphorylated phenols demonstrate both bridging and chelating behaviour, and the main reaction product is a coordination polymer containing dimeric Cu_2O_8 fragments. The structural peculiarities of the *o*-phosphorylated phenols were revealed by single-crystal X-ray diffraction. The copper complexes are studied by single-crystal and powder X-ray diffraction, and IR, Raman and X-ray photoelectron spectroscopy (XPS). The applicability of XPS spectroscopy to structural studies of coordination compounds with complex organic ligands is demonstrated with $Cu\mathbf{L^1}_2$ and $Cu\mathbf{L^2}_2$. The results of ab initio structure solution and Rietveld refinement of the $Cu\mathbf{L^2}_2$ structure from powder data are augmented by PW-PBE-D calculations.

Introduction

Aromatic *ortho*-phosphorylated phenols have attracted considerable attention as potential O,O-donor ligands with a broad set of possible substituents owing to their wide range of possible applications. For example, they have shown encouraging preliminary results as effective antenna in luminescent lanthanide complexes.[1] From the structural point of view, they can be considered as a distant relative of β-diketonates (Figure 1). It stands to reason that any level of conjugation is not expected for such a system, and this analogy is valid only as an illustrative example of structural conformity between both classes.

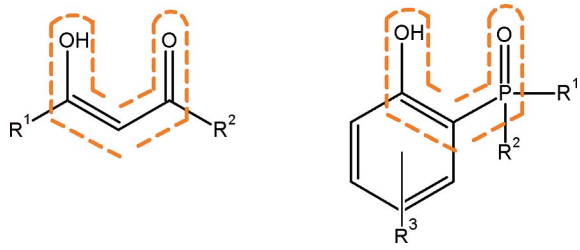

Figure 1. Structural conformity of the chelating part of enol β-diketonates (left) and *ortho*-phosphorylated phenols (right).

The structural mode of *ortho*-phosphorylated phenols in coordination compounds is still uncertain, and existing data is limited only to the synthesis of compounds without any structural data.[2–4] The main question is whether or not they can play the role of chelating or bridging ligands (Figure 2).

The ligand configuration is definitely influenced considerably by the chemical nature of the substituents (R^1 and R^2).

For this reason, we chose two ligands, (2-hydroxyphenyl)di-*p*-tolylphosphane oxide ($H\mathbf{L^1}$) and 3-(2-hydroxyphenyl)-3,4-dihydro-2*H*-benzo[*f*][1,5,3]dioxaphosphepine 3-oxide ($H\mathbf{L^2}$), with substituents with substantially different volumes (Figure 3).

As a starting point, copper(II) complexes were chosen to reveal the structural potential of the chosen ligands. Copper(II) forms the most stable complexes among 3d metals

[a] Department of Materials Science, Lomonosov Moscow State University,
119991 Moscow, Leninskie gory 1/3, Russia
Fax: +7-4959390998
E-mail: sergeyshuvaev@gmail.com
Homepage: http://www.inorg.chem.msu.ru/coord/
[b] A.N. Nesmeyanov Institute of Organoelement Compounds, Russian Academy of Sciences,
(INEOS RAS), GSP-1, 28 Vavilov Street, 119991 Moscow, Russia
[c] Laboratory of Industrial Chemistry, Ruhr-University Bochum, Universitätsstraße 150 44801 Bochum, Germany
[d] Institute of Physiologically Active Compounds, Russian Academy of Sciences,
142432 Chernogolovka, Severny proezd 1, Moscow Region, Russia
[e] Frumkin Institute of Physical Chemistry and Electrochemistry, Russian Academy of Sciences,
Leninsky Pr. 31, Moscow 119071, Russia

Supporting information for this article is available on the WWW under http://dx.doi.org/10.1002/ejic.201300540.

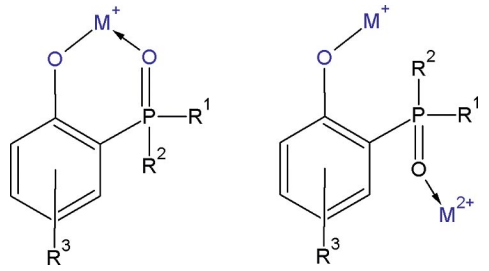

Figure 2. Two possible configurations of *o*-phosphorylated phenolate ligands. Left: chelating conformation. Right: bridging conformation.

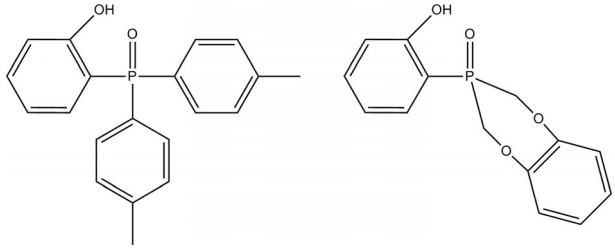

Figure 3. Aromatic *o*-phosphorylated phenols HL^1 (left) and HL^2 (right).

and demonstrates a clear tendency for square-planar coordination, such as in copper(II) β-diketonates.[5] Therefore, we can expect a similar coordination environment for aromatic *o*-phosphorylated phenols.

Thus, the main goal of present paper is the synthesis of copper complexes (CuL$^1_2$ and CuL$^2_2$) and the evaluation of the copper polyhedra by both X-ray diffraction and X-ray photoelectron spectroscopy. To the best of our knowledge, the latter approach has been infrequently used for the analysis of coordination compounds over recent decades.

Results and Discussion

Crystal Structures of *o*-Phosphorylated Phenols HL^1 and HL^2

To date, very little data is available on the crystal structures of aromatic *o*-phosphorylated phenols. Previously, the crystal structure of HL^2 was described, but that data needed additional verification owing to a relatively high *R* factor.[6] The mutual orientation of the P=O and C–O bonds (the O–C/P–O torsion angle) attracts particular interest as the flexibility of the O=P–C=C torsion angle directly affects the range of possible structures for coordination compounds containing these ligands.

The hydrogen-bond systems in the crystal structures of HL^1 and HL^2 are substantially different (Table S1). The unit cell of HL^1 contains two symmetrically independent molecules (HL^{1*} and HL$^{1\prime}$, Figure S3), which differ only slightly in the mutual orientation of the toluene substituent and the O1–P1–C1–C2 torsion angles [54.0(2) and –59.3(3)°, Figure S1]. Both molecules form intermolecular O–H···O=P hydrogen bonds. The crystal structure of HL^2 (Figure S4) is disordered and contains orientations of the 2-hydroxyphenyl group with O1–P1–C1–C2 torsion angles of 4.11(12) and 167.56(11)° in a ratio 0.54:0.46. In the former orientation, the OH group forms an intramolecular hydrogen bond with the P=O group [O···O 2.5407(15) Å, O–H···O 160.3(2)°], and in the latter it interacts with the P=O group of a neighbouring molecule [O···O 2.7182(13) Å, O–H···O 168.35(11)°]. Notably, in most β-diketone crystal structures, for example, that of dibenzoylmethane, only a strong intramolecular hydrogen bond is observed in the enol form,[7,8] which leads to an effective O–C···C–O torsion angle of 0. The *ortho*-phosphorylated phenols can be expected to be much more flexible ligands, as the corresponding average O–C···P=O torsion angles are 55.5° in HL^1 and either 2.2(2) or 162.7(2)° in HL^2.

Synthesis and Identification of Sodium Salts NaL^1 and NaL^2

o-Phosphorylated phenols HL^1 and HL^2 can be easily transformed into sodium salts by a simple reaction between HL and sodium hydroxide in methanol and isolated as solid products. The formation of NaL^1 and NaL^2 was confirmed by elemental analysis and by comparison of their spectral characteristics, including excitation and luminescence spectroscopy in both solution and powder forms, with those of HL^1 and HL^2. The ^{1}H NMR spectra demonstrate the disappearance of the "acidic" hydrogen atom of the hydroxy group, and the ^{31}P NMR spectra show a tangible upfield shift of the singlet resonances. At the same time, infrared and Raman spectroscopy revealed several splittings and shifts of the bands of the bonds mainly affected during deprotonation and introduction of sodium ions (P=O and C–O bonds). Both HL and NaL demonstrate luminescence in the near-UV region. From HL to NaL, a typical bathochromic shift was revealed (Figure S5), which indicates a decrease of the energy gap between the highest occupied molecular orbital (HOMO) and the lowest unoccupied molecular orbital (LUMO) by formation of sodium salts. Such a shift often accompanies a charge rearrangement in the molecular structure and is often observed during a change of bond type (e.g., if a predominantly covalent bond is substituted by an ionic bond as in saltlike structures).

Synthesis of Copper Complexes CuL$^1_2$, CuL$^1_2$·2MeOH and CuL$^2_2$

The copper complexes CuL$^1_2$ and CuL$^2_2$ were obtained by in situ reaction between freshly prepared solutions of the sodium salts in methanol and methanol solutions of $Cu(NO_3)_2 \cdot 2H_2O$. After slow evaporation of the methanol, greenish powders formed: a dark green amorphous precipitate of CuL$^1_2$, and a light green polycrystalline precipitate of CuL$^2_2$. To obtain CuL$^1_2$ in crystalline form, an alternative synthetic approach without the intermediate sodium salt was performed. The reaction between copper(II) acetate and HL^1 in *m*-xylene at reflux followed by the removal

of acetic acid by azeotropic distillation resulted in the formation of the same amorphous product CuL^1_2 and several single crystals of CuL^1_2·2MeOH as a byproduct isolated from the mother liquid. The structure of CuL^1_2·2MeOH was determined by single-crystal XRD (see Experimental Section), but the amount of it was too small to allow study by other methods. The CuL^2_2 specimen contained only one phase according to powder XRD, and its structure was determined from the powder data (see below). The complexes CuL^1_2 and CuL^2_2 were also identified by IR, Raman, diffuse-reflectance and X-ray photoelectron spectroscopy (XPS).

Structure of CuL^1_2 and CuL^2_2 Complexes

The structure of CuL^1_2·2MeOH contains a Cu atom with square-planar coordination. The Cu atom lies on an inversion centre; thus, the CuO_4 polyhedron has zero deviation from planarity. The Cu1–O1 and Cu2–O2 bond lengths are 1.9420(18) and 1.8951(19) Å, respectively (Figure 4). Such a coordination was an expected result for a β-diketonate analogue, but both the O 1s XPS and electron paramagnetic resonance (EPR) data for bulk CuL^1_2 disagree with this structure as it should be paramagnetic and contain two types of oxygen atoms in a 1:2 ratio (see below). The O–C···P=O torsion angle in this compound is 37.9(2)°, which shows that the analogy with β-diketonates is only superfluous. The bulk CuL^1_2 was amorphous according to the powder XRD data, and its crystal structure could not be determined directly. However, CuL^2_2 was crystalline and its structure was determined by ab initio methods from the powder diffraction data (see below). The structure was found to be a coordination polymer formed by CuL^2_2 chains along the *a* direction. The Cu atoms form dimeric Cu_2O_8 coordination polyhedra (on an inversion centre) that comprise two distorted CuO_5 square pyramids joined by a base edge. One ligand with an O–C···P=O torsion angle of 0.1(2)° provides the O2 atoms that bridge two CuO_5 pyramids, and the O1 atoms are the apexes of the pyramids. The other ligand forms a bridge between the dimeric Cu_2O_8 fragments with an O–C···P=O torsion angle of –101.1(2)°. Such coordination is unknown for β-diketonates but is fully in line with the flexibility demonstrated by the studied ligands in the uncoordinated form.

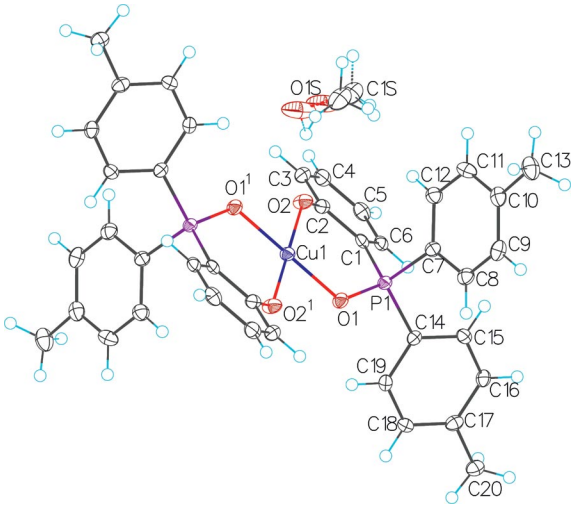

Figure 4. Overview of the CuL^1_2 crystal structure. Atoms are represented by thermal displacement ellipsoids (p = 50%), superscripts indicate symmetry-generated atoms and correspond to the following symmetry transformations. 1: $-x$, $-y$, $-z$. Only one disordered component of the methanol moiety is labelled.

As the geometry data obtained from the powder diffraction data often has low precision, we performed a PW-PBE-D DFT calculation for comparison. The deviation of the calculated result from the Rietveld refined structure was only 0.21 Å. The differences in the Cu–O bond lengths were more pronounced, as the Cu position was refined without any restraints, and are summarized in Table 1. Nevertheless, the geometry remained qualitatively the same, and the Cu–Cu distance allows spin coupling in line with the experimental EPR findings.

Table 1. The main bond lengths [Å] in the Rietveld refined and calculated structures of CuL^2_2.

	Rietveld refined	PW-PBE-D
Cu1–O2	1.89(3)	1.988
Cu1–O2A	1.88(2)	1.917
Cu1–O1A[a]	1.96(2)	1.973
Cu1–O1[b]	2.20(3)	2.371
Cu1–O2[b]	1.97(3)	2.000
Cu1–Cu1[b]	3.05(2)	3.172

[a] 3 – x, $-y$, $-z$. [b] 2 – x, $-y$, $-z$.

Determination of the Structure of CuL^2_2 from Powder XRD Data

The powder diffraction pattern (see Experimental Section) of CuL^2_2 was indexed by TOPAS 4.2 software[9] in the triclinic crystal system with the $P\bar{1}$ space group, as judged from the cell volume (expected Z' = 1). The lattice parameters (after Rietveld refinement) are a = 8.9008(3) Å, b = 10.6655(3) Å, c = 16.4108(8) Å, α = 103.660(4)°, β = 95.975(3)°, γ = 113.527(2)°, V = 1353.17(9) Å^3. The structure solution was performed by using the parallel-tempering method as implemented in FOX.[10] The model for the solution and refinement was prepared based on a PBE/L2[11] calculation of an isolated monomeric CuL^2_2 complex (analogous to the CuL^1_2 complex from CuL^1_2·2MeOH) by using PRIRODA.[12] The search with this model was unsuccessful, so two Cu–O bond constraints corresponding to Cu···O=P coordination, as well as C–O···Cu angle constraints, were removed, and the search was repeated. This search provided a reasonable position for one of the ligands and the Cu atom (one run out of 40), so that the Cu–O–Cu bridge and part of square Cu polyhedron could be identified. The final solution was obtained by constraining the Cu atom coordinates and the orientation and position of the ligand to the found ones, and searching for the position, conformation and orientation of the other ligand freely. The

resulting structure contained Cu atoms in 4+1 coordination polyhedra and was Rietveld refined in TOPAS 4.2 by using bond lengths and angles from the above model as restraints for the ligands. The Cu–O bond lengths and O–Cu–O angles were not restrained. Isotropic thermal parameters were refined independently for each atom type within each ligand, and the line-profile anisotropy was refined by using second order spherical harmonics.[13]

The "Morse" restraint model[14] was applied during the refinement (see Experimental Section). The analysis of the deviations of the refined bond lengths from the defined values within this restraint model has been shown to incorrectly identify the Rietveld refined structures. After 150 refinements in TOPAS with decreasing penalty function weight (K_1, see Experimental Section), there were no outliers in the bond-length-deviation (Δd) distribution (Figure 5), which further supports the accuracy of the refined structure (Figure 6). At K_1 = 8, the difference between the

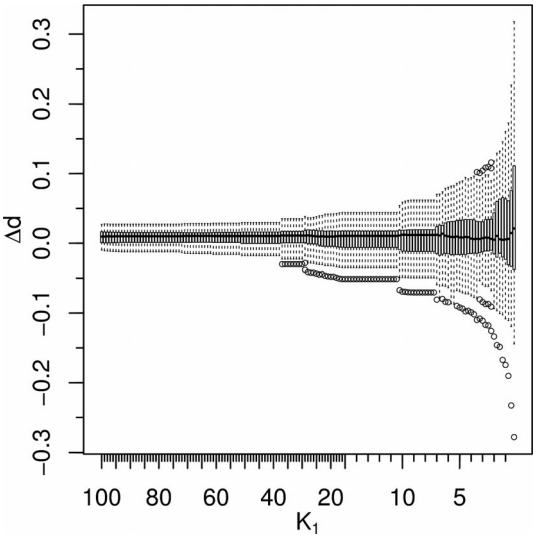

Figure 5. Multiple boxplot for Cu$\mathbf{L}^2_2$ Δd distributions at different values of K_1.

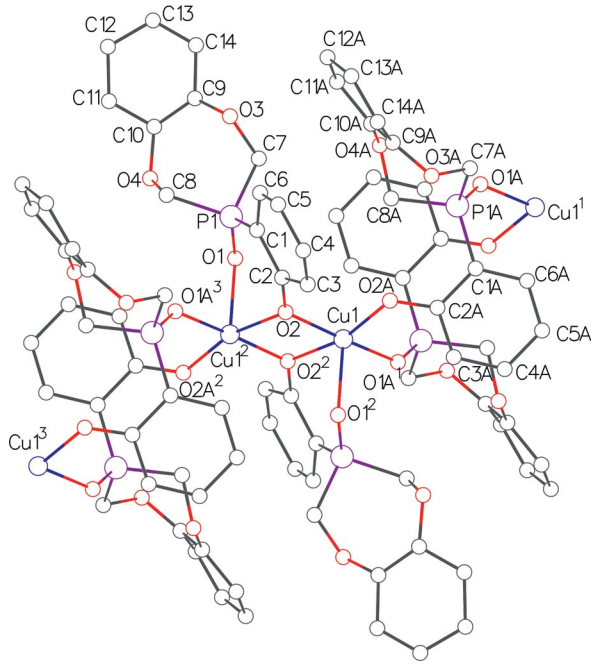

Figure 6. Overview of the Cu$\mathbf{L}^2_2$ crystal structure. Atoms are represented by spheres, superscripts indicate symmetry-generated atoms and correspond to the following symmetry transformations. 1: 3 – x, –y, –z; 2: 2 – x, –y, –z; 3: –1 + x, y, z.

Table 2. Refinement indicators for Pawley fit and Rietveld refinement of Cu$\mathbf{L}^2_2$.

	Pawley fit	Rietveld refinement
K_1	–	8
RMS Δd [Å]	–	0.029
R_{wp}[%]	2.37	2.62
R_{wp}' [%]	11.94	13.97
R_p [%]	1.66	1.91
R_p' [%]	12.49	16.07
R_{bragg} [%]	0.07	0.79
χ^2	2.28	2.17

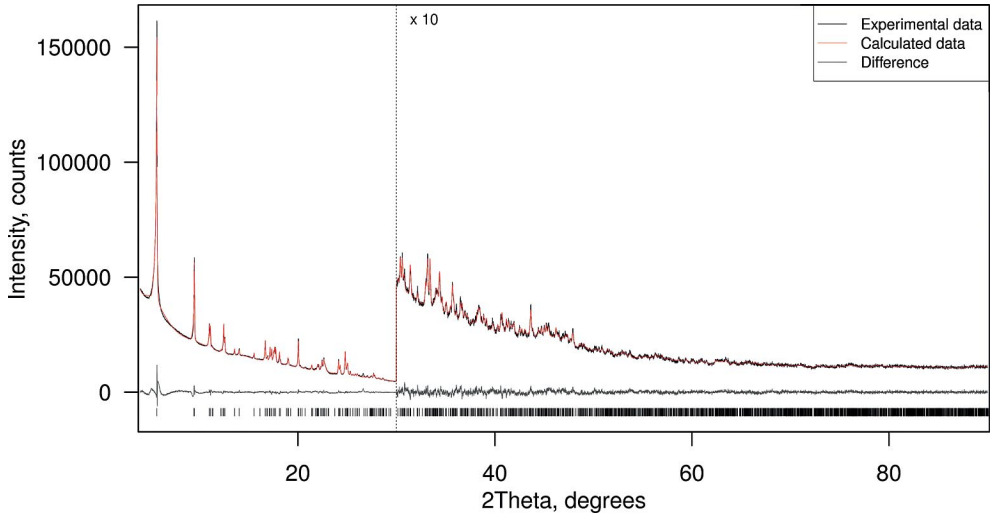

Figure 7. Calculated, experimental and difference powder patterns for Cu$\mathbf{L}^2_2$.

calculated and experimental patterns was featureless (Figure 7). A comparison between the final refinement indicators and those for a Pawley fit is summarized in Table 2.

Thermal Stability

To evaluate the thermal behaviour of the synthesized complexes, thermogravimetric/differential scanning calorimetry (TG-DSC) curves were recorded (Figure S6). Both complexes are thermally stable to ca. 190 °C, and their broad exothermic bands corresponding to the decomposition of complexes on the DSC curve are of similar shape.

Infrared and Raman Spectroscopy

Initial elucidation and assignment of the vibrational bands of the ligands were performed from theoretically calculated infrared and Raman spectra of HL^1 and HL^2. A preliminary comparison of the IR spectra of HL and CuL_2 (Figure S7) revealed considerable changes in the position and shape of the most important bands, ascribed to ν(P=O) and ν(C–O). For the P=O vibration modes, the most intense band centred at ca. 1120 cm^{-1} is observed in both complexes and contains at least two sub-bands (resolved for CuL^2_2 and unresolved for CuL^1_2). In addition to the ν(P=O) stretching mode, these bands comprise in-plane bending β(CCH) and stretching ν(C=C) of the aryl rings, as well as out-of-plane φ(HCH) twisting of the methylene bridges for HL^2 and CuL^2_2. In both cases (CuL^1_2 and CuL^2_2), the barycentre of these broad bands is slightly shifted towards lower frequencies, which is typical for coordinated P=O bonds.

For the bands corresponding to the C–O vibration mode, the best solution is to compare the obtained data with previous IR spectra of *ortho*-substituted phenols.[15] Here, we can single out two groups of bands corresponding to the C–O vibration modes. The first group centred at ca. 1245 cm^{-1} is unfavourable for analysis because of the overlap of the vibrations of several bonds. The second group centred at ca. 1305 cm^{-1} is considerably clearer for further analysis and, therefore, was chosen for comparison. In both cases, a broad band centred at ca. 1304 cm^{-1} comprising at least two sub-bands is observed, in contrast with the narrower bands revealed in the HL spectra. From theoretical calculations, for HL^2 and CuL^2_2 these bands are apparently the result of an overlap between ν_{symm}(C–C) of the catechol substituent with the in-plane bending β(OCH) and out-of-plane φ(HCH) wagging vibrations of the methylene bridges at lower frequencies, and ν(C–O) at higher frequencies, displayed as a shoulder. The lack of methylene bridges in HL^1 led to a narrower band comprising only ν_{symm}(C–C) and ν(C–O) vibrations. The nature of the additional band observed at higher frequencies for the copper complexes can be attributed to the two types of C–O bonds in the coordinated ligands (1.305 vs. 1.288 Å).

A relatively narrow band centred at 1420 cm^{-1} in the spectrum of HL^2, ascribed to in-plane β(COH) bending, disappears in the spectrum of CuL^2_2 and provides clear evidence of successful deprotonation.

A Raman spectrum was recorded only for CuL^2_2 (Figure 8), as CuL^1_2 melted under laser irradiation. Nevertheless, several maxima were determined and their values are listed below in the Experimental Section. The band corresponding to P=O vibration (ca. 1127 cm^{-1}) was substantially broadened and shifted towards higher energies (ca. 1159 cm^{-1}). The same shift is observed for the band ascribed to C–O bond vibration (ca. 1322 vs. ca. 1326 cm^{-1}). In addition, complexation affected the vibrational modes within the aromatic rings (several bands at ca. 1588 cm^{-1}).

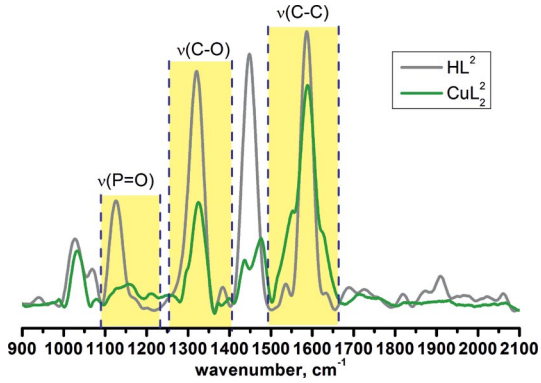

Figure 8. Raman spectra of HL^2 and CuL^2_2.

Diffuse-Reflectance Spectroscopy of CuL^1_2 and CuL^2_2

As CuL^1_2 is amorphous, absorption spectroscopy could be a useful tool in the determination of the copper polyhedra by comparison with the spectrum of CuL^2_2, for which the copper polyhedra are known. However, because of poor solubility, absorption spectroscopy in solution was substituted by diffuse-reflectance spectroscopy (Figure 9). The electronic absorption spectra contain two asymmetrical bands (one of them is unresolved for CuL^2_2) below 22000 cm^{-1} [attributed to d–d transitions of the copper(II) ions], which indicates the presence of more than one electronic transition with similar energy values (Figure 9).[16] The close proximity of the evaluated peak values and their

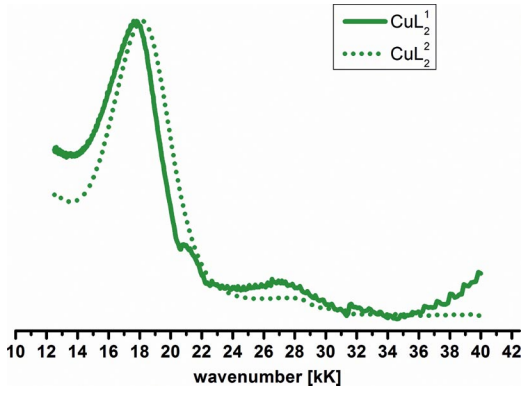

Figure 9. Diffuse-reflectance absorption spectra of CuL^1_2 and CuL^2_2 at ambient temperature.

shapes could indicate similar coordination polyhedra [viz. pentacoordinate copper(II) ions] and close ligand-field strength (LFS) values, in line with a minor impact of the substituents on the charge density localized on the oxygen atoms participating in complexation.[17] Broad bands at higher energies are ascribed to charge-transfer states and intraligand transitions.

X-ray Photoelectron Spectroscopy

To obtain a deeper insight into the coordination polyhedra around the copper(II) ions in amorphous Cu$\mathbf{L^1}_2$, XPS measurements were required. First, the XPS spectra of Cu$\mathbf{L^2}_2$ (with determined crystal structure) were recorded for use as a starting point for analysis of the spectrum of amorphous Cu$\mathbf{L^1}_2$ (with unknown structure of the copper polyhedra).

The C 1s photoelectron spectra of both Cu$\mathbf{L^1}_2$ and Cu$\mathbf{L^2}_2$ are presented on Figure S6. Both spectra demonstrate a major contribution at lower binding energies, which most likely belong to sp^2-hybridized aromatic carbon atoms and were referenced to 284.5 eV. The high-binding-energy components can be assigned to the sp^3-hybridized carbon atoms of substituent radicals [two methyl substituents for $(\mathbf{L^1})^-$ ligand and two methylene substituents for $(\mathbf{L^2})^-$] with 1:11.5 and 1:3 atomic ratios to the main aromatic fragments in the $(\mathbf{L^1})^-$ and $(\mathbf{L^2})^-$ samples, respectively. The latter ratio considerably contradicts the theoretical value (1:6) and could be explained by the formation of extra carbon in the X-ray beam from pump oil and other organic contamination on the surface of the samples.

Figure S9 shows the experimental P 2p photoelectron lines deconvoluted into a doublet with area ratio constrained according to p sublevel multiplicity (1:2). The P 2p 3/2 photoelectron lines are at slightly different binding energies, depending on the ligand nature (distinctions in P=O bond lengths). However, their energies (132.0 and 132.3 eV for Cu$\mathbf{L^1}_2$ and Cu$\mathbf{L^2}_2$, respectively) are close to the energies reported for phosphorus in different organic ligand surroundings.[18,19]

The Cu 2p photoelectron and Cu LMM X-ray Auger electron spectra (Figure 10, a and b, respectively) indicate that copper is present mostly in the 2+ oxidation state. There is also asymmetry in the Cu 2p 3/2 line for Cu$\mathbf{L^1}_2$ and an easily distinguishable shoulder on the high binding energy (BE) side of the Cu$\mathbf{L^2}_2$, which might indicate the presence of some other copper states. Unfortunately, the copper XPS signal was not intensive enough even after significant signal accumulation, so reliable signal deconvolution cannot be performed. The maxima of the Cu 2p 3/2 envelope position (934.0 and 933.7 eV for Cu$\mathbf{L^1}_2$ and Cu$\mathbf{L^2}_2$, respectively) and modified Auger[20] parameters values (1850.4 and 1850.7 eV) comply with those of copper 2+ reference compounds such as CuO.[21]

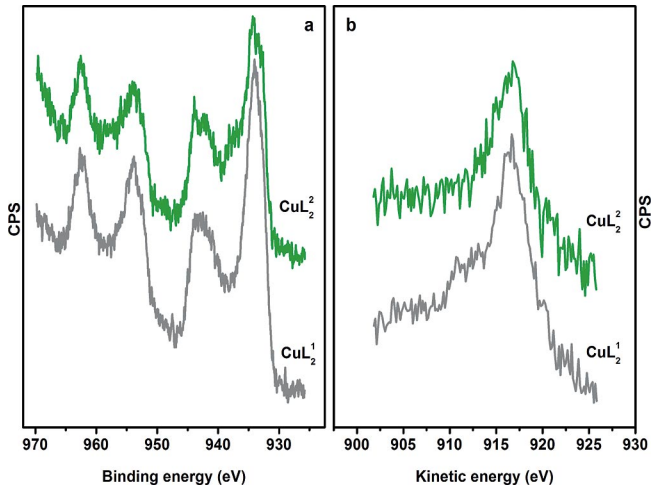

Figure 10. (a) Cu 2p photoelectron and (b) Cu LMM spectra.

The O 1s photoelectron spectra of both samples have major contributions at ca. 531.0 eV binding energy (Figure 11). These signals originate from the oxygen atoms that form the polyhedra around the copper ions. The spectrum of Cu$\mathbf{L^1}_2$ also shows a minor contribution at 532.4 eV binding energy, which most likely belongs to out-of-plane oxygen atoms in polyhedra around the copper ions (with a ratio between both contributions of 75:25). The O 1s photoelectron line of Cu$\mathbf{L^2}_2$ has a well-defined doublet structure, but it can be described by three contributions with a ratio of 50:37.5:12.5 positioned at 533.3, 531.0 and 531.8 eV binding energy, respectively, which is in a good agreement with the ratio between the in-plane and out-of-plane oxygen atoms in the polyhedra (1:3) of the obtained crystal structure. The contribution at 533.3 eV corresponds to the oxygen atoms of the dioxaphosphepine ring, and has a BE value that corresponds well to the literature data for C–O–Ph oxygen atoms in polymers (533.0–533.5 eV).[22] The line at 531.8 eV most likely corresponds to the O1 oxygen atom at the apex of the CuO_5 pyramid. As its bonding with Cu

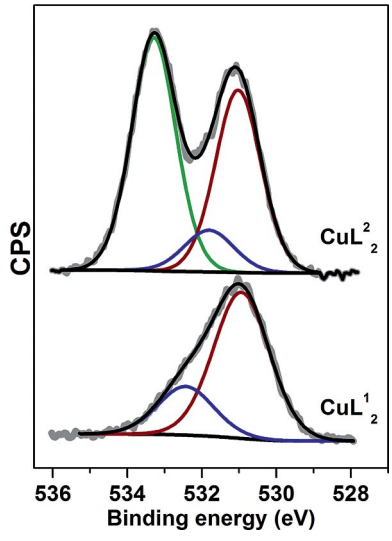

Figure 11. O 1s photoelectron spectra.

is relatively weak because of the significant Cu–O distance of 2.371 Å, its BE should be close to that of the oxygen atom in triphenylphosphine oxide (530.9–531.1 eV).[23]

In the XPS study, the most unexpected result obtained is the observation of high BE shoulders for the Cu 2p XPS lines. The binding energy for those contributions is rather high, ca. 937.0 eV; such values have only been reported for copper fluoride to date. One possible explanation for the extra signals would be a differential charging of the specimen surface. This effect is often observed when the sample has different parts with the same elements with different charges. The corresponding XPS lines have different shifts as a result. However, if that were the case, the shake-up satellites observed next to each of the Cu 2p lines would have the same extra contributions.

Additionally, it should be noted that the O 1s signal deconvolution performed for $Cu\mathbf{L^2}_2$ is not the only one possible, it is even not the simplest. The line envelope can be fitted with two Gaussian–Lorentz product components with the same goodness of fit. The present fit is a result of constraining the low BE component to 533.3 eV and using the expected intensity ratios. The same procedure can be performed by using the 531.0 eV component as the main one, which results in a shift of the minor component to higher BEs. A three-component model without constraints gives atomic ratios significantly different to the predicted ones, and the results strongly depend on the lineshape used (Gaussian and Lorentzian functions ratio). Therefore, the fact that the experimental signal shape can be reproduced with three components in the expected intensity ratio and plausible line shape parameters definitely lends experimental support to this ratio.

Electron Paramagnetic Resonance

To get additional data concerning the polyhedron around the copper ion in amorphous $Cu\mathbf{L^1}_2$, a comparison of the EPR spectra of both complexes ($Cu\mathbf{L^1}_2$ and $Cu\mathbf{L^2}_2$) is essential. For $Cu\mathbf{L^2}_2$, the close proximity between the copper ions within the dimeric fragment [3.05(2) Å] can give rise to coupling between the paramagnetic copper ions and overall diamagnetic behaviour. Actually, in both cases a signal was not detected (Figure S9), except for a slight contamination by a paramagnetic impurity in $Cu\mathbf{L^1}_2$, which was ascribed to a square-planar copper complex.[24] Therefore, for $Cu\mathbf{L^1}_2$, both types of coordination environment (square-planar and pentacoordinate) are present, but the pentacoordinate complex substantially prevails. The obtained results are entirely in line with our previous assumption about the proximity between both polyhedra ($Cu\mathbf{L^1}_2$ and $Cu\mathbf{L^2}_2$), and square-planar coordinated complexes were obtained only as a minor admixture.

Conclusions

The present paper aims to awake interest in the role of phosphorylated phenols as anionic ligands in coordination compounds. The crystal structures of the aromatic *ortho*-phosphorylated phenols $\mathbf{HL^1}$ and $\mathbf{HL^2}$ were determined, and the influence of substituents on packing motifs has been analyzed. Main distinctions were found in the mutual orientation of the P=O and C–O bonds and, as a result, the system of hydrogen bonds. In the crystal structures of the copper complexes ($Cu\mathbf{L^1}_2{\cdot}2MeOH$ and $Cu\mathbf{L^2}_2$), the mutual orientation of P=O and C–O bonds led to substantial distinctions in the type of polyhedra around the copper complex. Such a result clearly demonstrates that this type of prospective ligands can appear in both chelating and bridging modifications, depending on the chemical nature of substituents. One of the most significant results of this paper is the possibility to distinguish between different types of coordinated oxygen atoms by X-ray photoelectron spectroscopy.

Experimental Section

Materials: Analytically pure methanol and ethanol (Sigma–Aldrich), $Cu(NO_3)_2{\cdot}2H_2O$ and $Cu(CH_3COO)_2{\cdot}2H_2O$ (Riedel-de Haën) were used without further purification.

Measurements: The C, H and N contents were determined by conventional elemental analysis. IR spectra were recorded in the region 4000–400 cm^{-1} with a Perkin–Elmer Spectrum ONE FTIR spectrometer with samples in Nujol. Raman spectra were recorded in the region 400–2000 cm^{-1} by using a Renishaw InVia spectrometer. Diffuse-reflectance spectra were recorded in the region 250–800 nm with a Perkin–Elmer Lambda 650 spectrometer. Luminescence and excitation luminescence spectra were recorded in the region 200–450 nm with a Perkin–Elmer LS-55 spectrometer. ^1H and ^{31}P NMR spectra were obtained with a Bruker Avance-400 {400 MHz, [D_6]-DMSO/tetramethylsilane (TMS)} spectrometer. TG-DSC curves were obtained with a NETZSCH STA 409 PC/PG analyzer with argon flow at a heating rate of 10 °C/min in the temperature range 40–1000 °C.

Single-Crystal X-ray Diffraction (SC-XRD): X-ray quality single-crystals of $\mathbf{HL^1}$ and $\mathbf{HL^2}$ were grown by recrystallization from methanol solutions. The single-crystal X-ray diffraction data were collected with a Bruker SMART APEX II CCD diffractometer (Mo-K_α, λ = 0.71073 Å, graphite monochromator) at 100 K. The structures were solved by direct methods and refined with the full-matrix F^2 least-squares technique, as implemented in SHELX.[25] The hydrogen atoms of OH groups were found in difference Fourier syntheses. Other H atoms were placed in idealized positions and refined by using a riding model with fixed isotropic thermal parameters. The crystal data for the studied compounds is provided below.

$\mathbf{HL^1}$: $C_{20}H_{19}O_2P$ (M = 322.32): monoclinic, space group $P2_1/c$ (no. 14), a = 19.090(3) Å, b = 9.6266(14) Å, c = 18.199(3) Å, β = 90.332(3)°, V = 3344.4(8) $Å^3$, Z = 8, T = 100.0(2) K, μ(Mo-K_α) = 0.171 mm^{-1}, $D_{calcd.}$ = 1.280 g/mm^3, 22663 reflections measured ($2.24 \le 2\theta \le 56$), 7983 unique (R_{int} = 0.0472) reflections were used in all calculations. The final R_1 was 0.0550 [$I > 2\sigma(I)$] and wR_2 was 0.1525 (all data).

$\mathbf{HL^2}$: $C_{14}H_{13}O_4P$ (M = 276.21): monoclinic, space group $P2_1/n$ (no. 14), a = 9.7074(6) Å, b = 12.3078(7) Å, c = 10.7244(6) Å, β = 105.2600(10)°, V = 1236.14(12) $Å^3$, Z = 4, T = 100(2) K, μ(Mo-K_α) = 0.229 mm^{-1}, $D_{calcd.}$ = 1.484 g/mm^3, 12876 reflections measured ($5.04 \le 2\theta \le 60$), 3589 unique (R_{int} = 0.0512) reflections

were used in all calculations. The final R_1 was 0.0363 [$I > 2\sigma(I)$] and wR_2 was 0.1021 (all data).

CuL^1_2·2MeOH: $C_{42}H_{44}CuO_6P_2$ (M = 770.25): triclinic, space group $P\bar{1}$ (no. 2), a = 9.325(2) Å, b = 10.057(2) Å, c = 10.099(2) Å, α = 99.686(5)°, β = 93.142(5)°, γ = 103.912(5)°, V = 901.7(4) Å^3, Z = 1, T = 100(2) K, μ(Mo-K_α) = 0.744 mm^{-1}, $D_{calcd.}$ = 1.418 g/mm^3, 10799 reflections measured (4.12 ≤ 2θ ≤ 58), 4780 unique (R_{int} = 0.0526) reflections were used in all calculations. The final R_1 was 0.0482 [$I > 2\sigma(I)$] and wR_2 was 0.1199 (all data).

X-ray Powder Diffraction (XRD): The powder pattern of CuL^2_2 was measured with a Bruker D8 Advance Vario diffractometer with a LynxEye detector and Ge (111) monochromator, λ(Cu-K_α1) = 1.54060 Å, $\theta/2\theta$ scan from 4 to 90°, stepsize 0.0104788°. The measurement was performed in transmission mode with CuL^2_2 deposited on kapton film.

The penalty function in the "Morse" restrained refinement is defined as follows:

$$P = K_1 \sum_i \kappa_i [1 - e^{-a_i(D_i - d_i)}]^2$$

in which P is penalty function, K_1 is a global penalty function weighting, κ_i is the weighting of the individual bond penalty, a_i is a coefficient corresponding to the bond force constant, D_i is the defined length of a given bond and d_i is its refined length at current minimization step.

Periodic Density Functional Calculation of CuL^2_2: Periodic DFT calculations of crystal structures CuL^2_2 were performed by using the VASP 5.212 code.[26–29] The conjugated-gradient technique was used for optimizations of the atomic positions and minimization of the total energy. Experimental atomic coordinates (with K_1 = 8) and the cell parameters of CuL^2_2 were taken as the starting point. The projected augmented wave (PAW) method was applied to account for core electrons, and valence electrons were approximated by plane-wave expansion with a 400 eV cutoff. Exchange and correlation terms of total energy were described by a PBE exchange-correlation functional.[30] Kohn–Sham equations were integrated by using a Γ-point approximation with additional dispersion correction.[31] At the final step of our calculations, the atomic displacements converged better than 0.03 eV Å^{-1}, and the energy variations were less than 10^{-4} eV. The atomic coordinates for the calculations can be found in the Supporting Information.

CCDC-935792 (for HL^1), -935793 (for HL^2), -935794 (for CuL^1_2·2MeOH) and -935795 (for CuL^2_2) contain the supplementary crystallographic data for this paper. These data can be obtained free of charge from The Cambridge Crystallographic Data Centre via www.ccdc.cam.ac.uk/data_request/cif.

X-ray Photoelectron Spectroscopy (XPS): Measurements were performed in an ultra-high vacuum (UHV) set-up equipped with a monochromatic Al-K_a X-ray source ($h\nu$ = 1486.6 eV), operated at 14.5 kV and 35 mA, and a high-resolution Gammadata-Scienta SES 2002 analyzer. The base pressure in the measurement chamber was maintained at ca. 7× 10^{-10} bar. The measurements were performed in the fixed transmission mode with a pass energy of 200 eV resulting in an overall energy resolution of 0.25 eV. A flood gun was applied to compensate the charging effects. High-resolution spectra for C 1s, O 1s, Cu 2p and P 2p photoelectron lines along with Cu LMM Auger transitions were recorded. The binding-energy scales were corrected to the charge shift by referencing the most intensive sp2-hybridized C 1s contribution to 284.5 eV. The Casa XPS software with a Gaussian–Lorentzian product function and Shirley background subtraction was used for peak deconvolution.

Theoretical Calculation of Infrared and Raman Spectra: The structures of initial molecules HL^1 and HL^2 were optimized at the B3LYP/6-311*G+ level[32,33] by using the Gaussian 09 package. The infrared and Raman intensities were calculated for optimized geometries in the framework of the same DFT method. All theoretically calculated frequencies were be real, which indicates the true minimum of the calculated total energy. To provide an easier comparison with experimental spectra, a scaling factor of 0.975 was introduced. Vibrational assignment of fundamental modes was performed on the ground of the calculated vibrational mode animation with the ChemCraft program.

Electron Paramagnetic Resonance (EPR): The measurements were performed with a Varian E-4 X-band ($\nu \approx$ 9.1 GHz) EPR spectrometer. The temperature measurements were performed with the use of a platinum resistor transducer (50 Ω at 0 °C) with an accuracy of ±0.5 K.

Syntheses: Aromatic *o*-phosphorylated phenols (HL^1 and HL^2) were synthesized according to the synthetic route described elsewhere.[5] The purity of the synthesized compounds was proved by C, H, N analysis and ^{1}H and ^{31}P NMR spectroscopy.

A mixture of HL and NaOH (1:1) was prepared in methanol solution with stirring and heating at 60 °C for 1 h. Afterwards, a white precipitate was isolated in good yield (85%) after slow evaporation of the solvent over several days at room temperature. The isolated product was identified by C,H,N analysis, ^{1}H and ^{31}P NMR spectroscopy and IR spectroscopy.

NaL^1: IR: $\tilde{\nu}$ = 1116 (s), 1148 (m, P=O), 1163 (m), 1243 (w), 1267 (m, C–O), 1440 (s, P–C) cm^{-1}. ^{1}H NMR: δ = 2.40 (s, 6 H, Me), 6.84 (2× d, 2 H, OPh), 7.23 (t, 1 H, OPh), 7.27 (2× d, 4 H, Ph), 7.36 (t, 1 H, OPh), 7.50 (q, 4 H, Ph) ppm. ^{31}P NMR: δ = 27.91 (s) ppm. $C_{20}H_{18}NaO_2P$ (344.32): calcd. C 69.77, H 5.23; found C 69.58, H 5.37.

NaL^2: IR: $\tilde{\nu}$ = 1126 (m), 1168 (m, P=O), 1250 (m, C–O), 1429 (m, P–C), 1445 (s), 1453 (s), 1489 (s) cm^{-1}. ^{1}H NMR: δ = 4.70–4.75 (2× d, $J_{H,H}$ = 14.65, 14.78 Hz, $J_{P,H}$ = 7.07, 7.20 Hz, 2 H, CH_2), 4.97–5.01 (d, $J_{H,H}$ = 14.66 Hz, $J_{P,H}$ = 1.14 Hz, 2 H, CH_2), 6.84 (2× d, 2 H, OPh), 7.23 (t, 1 H, OPh), 7.27 (2× d, 4 H, Ph), 7.42–7.46 (t, $J_{H,H}$ = 7.96, 7.57 Hz, 1 H, OPh), 7.66–7.71 (t, $J_{H,H}$ = 9.17, 9.58 Hz, 1 H, OPh) ppm. ^{31}P NMR: δ = 35.75 (s) ppm. $C_{14}H_{12}NaO_4P$ (298.21): calcd. C 56.39, H 4.06; found C 56.24, H 4.15.

$Cu(NO_3)_2$·$2H_2O$ (0.31 mmol) was added to a mixture of HL and NaOH in ethanol (molar ratio 1:2:2), and the mixture was stirred for 1 h at ambient pressure. After evaporation of the solvent in air, green precipitates of different tints were isolated, rinsed with distilled water and dried in air over one day, yield ca. 80%. Notably, the hydrate content of the isolated precipitates (amorphous for CuL^1_2 and polycrystalline for CuL^2_2) is not the same for both complexes. Both CuL^1_2 and CuL^2_2 were unsolvated without further drying.

$Cu(CH_3COO)_2$·$2H_2O$ (0.31 mmol) was dissolved in methanol and added to HL^1 in *m*-xylene (molar ration 1:2). The mixture was heated to reflux for 4 h, and the acetic acid was subsequently removed by azeotropic distillation. After evaporation of the solvent in air, a dark green amorphous precipitate was isolated, rinsed with distilled water and dried in air for one day, yield ca. 80%.

CuL^1_2: $C_{40}H_{38}CuO_4P_2$ (708.23): calcd. C 68.03, H 5.14; found C 67.87, H 5.19. IR: $\tilde{\nu}$ = 1118 (vs, P=O), 1161 (w), 1248 (m), 1266 (m, C–O), 1437 (vs, P–C) cm^{-1}. Raman: $\tilde{\nu}$ = 1030, 1128, 1334, 1446, 1461, 1589 cm^{-1}.

CuL^2_2: $C_{28}H_{24}CuO_8P_2$ (613.99): calcd. C 54.77, H 3.94; found C 55.01, H 3.83. IR: $\tilde{\nu}$ = 1118 (s, P=O), 1136 (s), 1167 (m), 1238 (m), 1251 (s, C–O), 1435 (s, P–C) cm^{-1}. Raman: $\tilde{\nu}$ = 1029, 1311, 1333, 1440, 1472, 1588 cm^{-1}.

Supporting Information (see footnote on the first page of this article): molecular and crystal structures of HL^1 and HL^2; hydrogen-bond parameters of HL^1 and HL^2; luminescence and luminescence excitation spectra of HL^1, HL^2, NaL^1 and NaL^2; IR spectra of HL^1, HL^2, CuL^1_2 and CuL^2_2; C 1s and P 2p XPS spectra of CuL^1_2 and CuL^2_2; TG-DSC curves of CuL^1_2 and CuL^2_2; EPR spectra of CuL^1_2 and CuL^2_2.

Acknowledgments

The authors thank Dr. Vladimir Dolzhenko of the Inorganic Chemistry Department (MSU), Dr. Dmitry Tsymbarenko of the Material Sciences Department (MSU) and Mr. Dmitry Gil of the Kurnakov Institute of general and inorganic chemistry of the Russian Academy of Sciences. This study was partially supported by Russian Foundation for Basic Research (grant numbers 12-03-31560, 12-03-33107 and 12-03-00878-a).

[1] S. Shuvaev, O. Kotova, V. Utochnikova, A. Vaschenko, L. Puntus, V. Baulin, N. Kuzmina, A. Tzivadze, *Inorg. Chem. Commun.* **2012**, *20*, 73–76.
[2] K. A. Petrov, V. M. Chizhov, V. P. Pokatun, S. V. Agafonov, *Russ. Chem. Rev.* **1986**, *55*, 1042–1053.
[3] V. I. Evreinov, V. E. Baulin, Z. N. Vostroknutova, Z. V. Safronova, I. B. Krashakova, *Bull. Acad. Sci. USSR Div. Chem. Sci. (Engl. Transl.)* **1992**, *40*, 1759–1766.
[4] G. I. Bondarenko, *J. Struct. Chem.* **1996**, *37*, 206–209.
[5] R. C. Mehrotra, R. Bohra, D. P. Gaur, in: *Metal β-diketonates and allied derivatives*, Academic Press, London, **1978**.
[6] E. N. Zvetkov, V. H. Sundukova, V. E. Baulin, *Bull. Acad. Sci. USSR Div. Chem. Sci. (Engl. Transl.)* **1989**, *38*, 135–137.
[7] S. Öztürk, M. Akkurt, S. İde, *Cryst. Mater.* **1997**, *212*, 808–810.
[8] N. V. Belova, H. Oberhammer, G. V. Girichev, *Struct. Chem.* **2011**, *22*, 269–277.
[9] Bruker, *TOPAS*, v. 4.2, *User Manual*, Bruker AXS GmbH, Karlsruhe, Germany, **2009**.
[10] V. Favre-Nicolin, R. Černý, *J. Appl. Crystallogr.* **2002**, *35*, 734–743.
[11] D. N. Laikov, *Chem. Phys. Lett.* **2005**, *416*, 116–120.
[12] D. N. Laikov, *Chem. Phys. Lett.* **1997**, *281*, 151–156.
[13] M. Järvinen, *J. Appl. Crystallogr.* **1993**, *26*, 525–531.
[14] I. S. Bushmarinov, A. O. Dmitrienko, A. A. Korlyukov, M. Yu. Antipin, *J. Appl. Crystallogr.* **2012**, *45*, 1187–1197.
[15] Z. Rappoport, in: *The chemistry of phenols*, Wiley-VCH, Weinheim, Germany, **2003**, p. 333–395.
[16] N. A. Rey, A. Neves, A. J. Bortoluzzi, W. Haase, Z. Tomkowicz, *Dalton Trans.* **2012**, *41*, 7196–7200.
[17] Z. D. Matović, B. Ristić, M. Joksović, S. R. Trifunović, G. Pelosi, S. Ianelli, G. Ponticelli, *Transition Met. Chem.* **2000**, *25*, 720–726.
[18] W. E. Morgan, W. J. Stec, R. G. Albridge, J. R. van Wazer, *Inorg. Chem.* **1971**, *10*, 926–930.
[19] M. Pelavin, D. N. Hendrickson, J. M. Hollander, W. L. Jolly, *J. Phys. Chem.* **1970**, *74*, 1116–1121.
[20] C. D. Wagner, L. H. Gale, R. H. Raymond, *Anal. Chem.* **1979**, *51*, 466–482.
[21] C. D. Wagner W. M. Riggs L. E. Davis J. F. Moulder, G. E. Muilenberg, in: *Handbook of X-ray Photoelectron Spectroscopy*, Perkin–Elmer Corporation, Physical Electronics Division, Eden Prairie, **1979**.
[22] D. Briggs, G. Beamson, *Anal. Chem.* **1993**, *65*, 1517–1523.
[23] W. E. Morgan, W. Stec, R. G. Albridge, J. R. Van Wazer, *Inorg. Chem.* **1971**, *10*, 926–930.
[24] J. R. Pilbrow, *Transition Ion Electron Paramagnetic Resonance*, Calendron Press, Oxford, **1990**.
[25] G. M. Sheldrick, *SHELXL97*, *Program package for crystal structure determination*, University of Göttingen, Germany, **1998**.
[26] G. Kresse, J. Furthmüller, *Comput. Mater. Sci.* **1996**, *6*, 15–50.
[27] G. Kresse, J. Furthmüller, *Phys. Rev. B* **1996**, *54*, 11169–11186.
[28] G. Kresse, J. Hafner, *Phys. Rev. B* **1993**, *47*, 558–561.
[29] G. Kresse, J. Hafner, *Phys. Rev. B* **1994**, *49*, 14251–14269.
[30] J. P. Perdew, K. Burke, M. Ernzerhof, *Phys. Rev. Lett.* **1996**, *77*, 3865–3868.
[31] S. Grimme, *J. Comput. Chem.* **2006**, *27*, 1787–1799.
[32] A. D. Becke, *J. Chem. Phys.* **1993**, *98*, 5648–5652.
[33] C. Lee, W. Yang, R. G. Parr, *Phys. Rev.* **1988**, *37*, 785–789.

Received: April 24, 2013
Published Online: ■

